Positive-Net-Damping Stability Criterion in Grid-Connected VSC Systems

L. Sainz, M. Cheah-Mane, Ll. Monjo, J. Liang, O. Gomis-Bellmunt

Abstract- **Resonance instabilities in power systems can be assessed with the positive-net-damping stability criterion. This criterion is a review of the complex torque coefficients method but it does not provide the frequency of the closed-loop oscillatory modes. This paper presents an alternative approach of the positive-net-damping stability criterion to analyze electrical resonance instability. In this approach, resonance instabilities are identified in feedback systems derived from impedance-based equivalent circuits. The proposed approach is used to characterize the frequency of closed-loop oscillatory modes and identify the physical and control parameters of the system that increase or reduce the damping of these modes. The extension of the proposed approach to study the stability of Single-Input Single-Output and Multiple-Input Multiple-Output feedback systems is analyzed and the approach is also compared with other stability methods in the literature. An example of an offshore wind power plant illustrates the theoretical study and compares the proposed approach with different methods to evaluate stability. Time-domain simulations in PSCAD/EMTDC are shown to validate the stability study.**

Index Terms— **Electrical resonance, voltage stability, voltage source converters.**

I. INTRODUCTION

Grid-connected voltage source converters (VSCs) are widely used in renewable energy conversion systems (variable speed wind turbines and photovoltaics) and energy storage systems to improve controllability of power systems (e.g., microgrids [1] and wind power plants (WPPs) [2], [3]). However, resonance instabilities can appear in poorly damped power systems due to interaction between VSC control and the grid. In general, these resonance instabilities can be classified in two categories [4]: (i) Harmonic resonance instabilities which approximately range from 0.75 to 2 kHz and are caused by negative dampings due to VSC time delay and current control dynamics. (ii) Near-synchronous resonance instabilities which approximately range from 50 to 300 Hz and are caused by negative dampings due to current control dynamics and outer controls. The harmonic resonance instabilities are reported in different grid-connected VSC applications such as single-phase ac traction systems [6] and WPPs [7]. Also, a

number of methods to analyze resonance stability are reported in the literature [4], [8] − [19]. A good method is expected to have the following characteristics: (i) be simple to evaluate and compute, (ii) offer the possibility to assess stability from measurements and not requiring detailed knowledge of the system, (iii) provide enough information to understand physically instabilities and their causes and (iv) characterize the frequency of closed-loop unstable oscillatory modes.

The state space eigenvalue analysis (or closed-loop root study) and frequency domain methods are used to analyze the impact of system and control parameters on stability [8] − [13]. The Nyquist criterion and the phase and gain margin from the Bode diagram are the most used frequency domain methods to determine stability [9] − [13]. Other frequency domain methods are based on the impedance characterization of the system which allows considering the individual contribution that source and load subsystems have on the closed-loop stability [4], [9] − [20]. The passivity-based method ensures that a closed-loop system is stable if the real part of each subsystem is non-negative for all frequencies [4], [13], [14]. This method imposes passivity on all system elements to achieve stability but the non-passivity of a subsystem does not necessarily mean that the system is unstable. On the other hand, the following methods derived from the Nyquist criterion consider the stability contribution of each subsystem even when they are not passive:

- The impedance-based stability criterion [10] − [12] evaluates the phase of the open-loop functions at frequencies where the open-loop magnitudes intersect.
- The positive-net-damping stability criterion [19], [20] evaluates the net damping of the system at frequencies where the loop gain is greater than 1 as well as at frequencies of each open-loop resonance. This criterion is proposed by [20] to review the complex torque coefficients method [15] − [18] which is applied to study subsynchronous torsional interactions of turbine-generator sets [15], [16].

The impedance-based stability criterion provides information on the frequency of the closed-loop oscillatory modes from the frequency of the open-loop magnitude intersection while the positive-net-damping stability criterion only provides information on the frequency range of these oscillatory modes. The positive-net-damping stability criterion focuses on the net damping (i.e., the sum of the source and load resistances or conductances) while the impedance-based

L. Sainz and O. Gomis-Bellmunt are with the Dep. of Electrical Eng., UPC, Av. Diagonal 647, 08028 Barcelona, Spain (mail: sainz@ee.upc.edu, oriol.gomis@upc.edu). Ll. Monjo is with the Dep. of Industrial and Design System Eng., Univ. Jaume I, Av. de Vicent Sos Baynat, s/n, 12071 Castelló de la Plana, Spain (mail: lmonjo@uji.es). M. Cheah-Mané and J. Liang are with the School of Engineering, Cardiff University, CF24 3AA, Cardiff, U.K. (mail: CheahM@cardiff.ac.uk, LiangJ1@cf.ac.uk)
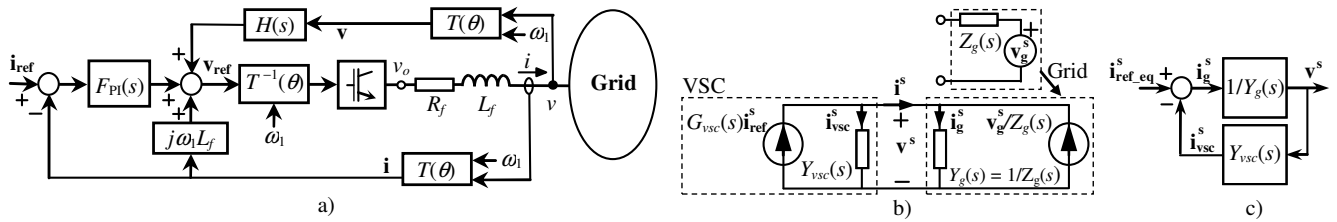
Fig. 1. Grid-connected VSC system modeling: a) Grid-connected VSC system. b) Equivalent circuit. c) Closed-loop system.

stability criterion focuses on the phase margin of the source and load impedance ratio. A recent study based on the complex torque coefficients method investigates near-synchronous resonance instabilities in grid-connected VSC systems from the analysis of the damping at the closed-loop oscillatory modes [21]. The damping is also used in [22] to study stability in weak grid-connected VSC systems. The conclusions in [22] are graphically obtained from the damping evaluation using the phase of the system transfer function instead of the real part of this function.

This paper presents and mathematically demonstrates an alternative approach to the positive-net-damping stability criterion in order to study harmonic resonance instabilities in grid-connected VSC systems. This approach meets the advantages of the impedance-based stability criterion (it allows characterizing the frequency of closed-loop oscillatory modes) and the positive-net-damping stability criterion (it allows identifying the physical and control parameters of the system that increase or reduce the damping of the closed-loop oscillatory modes). The approach is also compared analytically and numerically with other methods in the literature. Moreover, the extension of the proposed approach to assess the stability of Single-Input Single-Output (SISO) and Multiple-Input Multiple-Output (MIMO) feedback systems is discussed. An example of an offshore WPP illustrates the application of this criterion. The analytical and numerical results are validated by time-domain simulations in PSCAD/EMTDC.

II. GRID-CONNECTED VSC MODELING

Fig. 1(a) presents a grid-connected VSC system where the grid can include the effect of other VSCs. The dq-frame PI-based current control of the VSC is explicitly illustrated with bold letters denoting the complex space vectors (i.e., $\mathbf{x} = x_d + j \cdot x_q$) [13]. These space vectors are related to the grid components of angular fundamental (synchronous) frequency $\omega_1 = 2\pi \cdot f_1$ by means of the corresponding transfer matrices. It must be noted that the converter model in this Section only represents the inner current control loop because the outer loops (e.g., the phase-locked loop, PLL, and the direct-voltage controller, DVC) do not affect harmonic resonance instabilities in the 0.75 kHz to 2 kHz frequency range due to their low bandwidths [4], [5]. It can be observed that the transfer matrices of the VSC model in [14] become the common diagonal matrices of the VSC inner current control loop for frequencies greater than the low bandwidths of the outer

control loops. A symmetrical VSC model is obtained from this assumption and this model can be characterized with complex impedances or admittances. If outer loops are included, the system becomes nonlinear and VSCs must be represented by real vectors and transfer matrices leading to a two-dimensional MIMO model [23].

A. VSC model

The VSC current control model is obtained from the voltage balance across the converter filter,

$$\mathbf{v_o} = (R_f + L_f s + jL_f \omega_1)\mathbf{i} + \mathbf{v},\tag{1}$$

and the control law

$$\mathbf{v_{ref}} = F_{PI}(s)(\mathbf{i_{ref}} - \mathbf{i}) + jL_f \omega_1 \mathbf{i} + H(s)\mathbf{v},\tag{2}$$

where $\mathbf{v}$ and $\mathbf{i}$ are the grid voltage and current, $\mathbf{v_o}$ is the converter output voltage, $\mathbf{v_{ref}}$ and $\mathbf{i_{ref}}$ are the converter voltage and current reference and $F_{PI}(s)$ and $H(s)$ are the transfer functions of the feedback PI controller and the grid voltage feedforward low-pass filter included in the control,

$$F_{PI}(s) = k_p + \frac{k_i}{s} \qquad H(s) = \frac{\alpha_f}{s + \alpha_f},\tag{3}$$

with k_p and k_i being the PI controller proportional and integral gains, respectively, and α_f (or $f_f = \alpha_f/(2\pi)$) the low-pass filter bandwidth. Based on [14], the control design results in $k_p = \alpha_c L_f$ and $k_i = \alpha_c R_f$ where α_c is the closed current control loop bandwidth which should verify $\alpha_c \leq 0.2 \cdot (2\pi f_{sw})$ with f_{sw} being the converter switching frequency. The selection of the low-pass filter bandwidth is a compromise between the stability of the VSC output and the whole system stability [2], [13], [14], [22]. A small value of this bandwidth is used to keep as narrow as possible the VSC non-passivity region and improve the VSC stability. On the other hand, a large value is required to improve dynamics during fast transients due to grid disturbances that affect stability of VSC terminal voltage. The recommended low-pass filter bandwidth is $\alpha_f \leq 0.1\alpha_c$ for normal-mode operation and $\alpha_f \geq \alpha_c$ for transient-mode operation [14]. If VSCs are connected to a stiff bus, the feedforward low-pass filter design $\alpha_f \leq 0.1\alpha_c$ ensures that current from the converter is stable [14]. If VSC connects to a weak grid, the feedforward low-pass filter design $\alpha_f \geq \alpha_c$ ensures that the terminal voltage is stable in case of grid disturbances [2], [22].

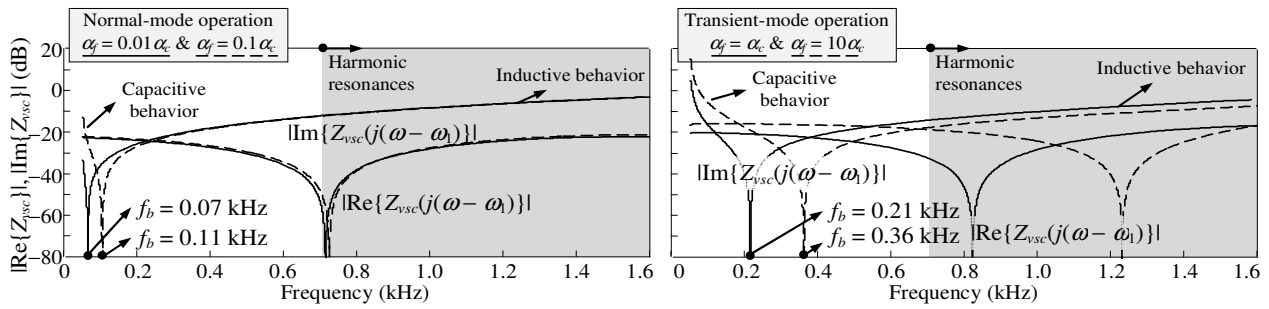The voltage $\mathbf{v_o}$ generated by the VSC is related to the

Fig. 2. Study of the VSC equivalent impedance response.

converter voltage reference $\mathbf{v_{ref}}$ considering the VSC time delay T_d as follows [4]:

$$\mathbf{v_o} = e^{-sT_d}\mathbf{v_{ref}}. \qquad (4)$$

This time delay is caused by the computation and the switching process and is approximately given by $T_d \approx 1.5T_s$ with $T_s = 1/f_s$ and f_s being the converter sampling frequency which is assumed twice the converter switching frequency [4]. Considering (4), the following relation between the grid voltage and current is obtained from (1) and (2):

$$\mathbf{i} = G_{vsc}(s)\mathbf{i_{ref}} - Y_{vsc}(s)\mathbf{v}, \qquad (5)$$

with

$$G_{vsc}(s) = \frac{e^{-sT_d}F_{PI}(s)}{R_f + L_f s + jL_f\omega_1 + e^{-sT_d}(F_{PI}(s) - jL_f\omega_1)}$$

$$Y_{vsc}(s) = \frac{1 - e^{-sT_d}H(s)}{R_f + L_f s + jL_f\omega_1 + e^{-sT_d}(F_{PI}(s) - jL_f\omega_1)}. \qquad (6)$$

where $G_{vsc}(s)$ is the closed-loop transfer function and $Y_{vsc}(s)$ is the equivalent admittance of the VSC.

Fig. 2 illustrates the frequency response of the positive-sequence VSC equivalent impedance in $\alpha\beta$-frame, i.e., $Z_{vsc}(s) = 1/Y_{vsc}(s)$ (6) with $s = j(\omega - \omega_1)$ [11], for the parameter values in Table I and four values of the low-pass filter bandwidth corresponding to normal-mode operation ($\alpha_f = 0.01\alpha_c$ and $\alpha_f = 0.1\alpha_c$) and transient-mode operation ($\alpha_f = \alpha_c$ and $\alpha_f = 10\alpha_c$). The frequency range of the harmonic resonance frequencies is also indicated in grey color [4]. It can be observed that for usual values of VSC parameters the VSC equivalent impedance presents a capacitive and an inductive response below and above the boundary frequency f_b, respectively[12]. It can also be observed that the response

above the boundary frequency f_b is mainly inductive due to the low contribution of the VSC resistive response. Thus, the VSC equivalent impedance at harmonic resonance instability frequencies is mainly inductive [12] because these frequencies are greater than the boundary frequency [4], [5].

B. Grid-connected VSC model

Considering the above VSC model, the impedance-based equivalent circuit of the grid-connected VSC system is shown in Fig. 1(b), where the VSC is represented as a current source in parallel with the equivalent VSC admittance, and the grid (characterized as stiff − or ideal − voltage source $\mathbf{v_g}$ in series with the grid equivalent impedance $Z_g(s)$) is also modeled as a current source $\mathbf{v_g}/Z_g(s)$ in parallel with the grid equivalent admittance $Y_g(s) = 1/Z_g(s)$. The resistive elements of the ac grids are usually neglected compared to the reactive elements and the impedance $Z_g(s)$ is commonly characterized by reactances in harmonic resonance studies [12], [14], [21]. It must be noted that the grid and VSC transfer functions are in phase and dq coordinates, respectively, and they must be in the same frame in Fig. 1(b) to evaluate stability. For that, both transfer functions are expressed in $\alpha\beta$ coordinates with bold letters denoting the space vectors and superscript $\mathbf{s}$ denoting the $\alpha\beta$-frame (i.e., $\mathbf{x^s} = x_\alpha + j \cdot x_\beta$). The VSC closed-loop transfer function and equivalent admittance in (6) are transformed from dq coordinates to $\alpha\beta$ coordinates by means of the frequency translation $s \rightarrow s - j\omega_1$ and the grid transfer function in phase coordinates is the same as in $\alpha\beta$ coordinates [18], [23].

The impedance-based equivalent circuit in Fig. 1(b) can also be represented as the closed-loop system in Fig. 1(c), [10], [11], which is obtained from the transfer function between the sources and the grid voltage $\mathbf{v^s}$ (or current $\mathbf{i^s}$) as follows:

$$\mathbf{v^s} = Z_t(s)\mathbf{i^s_{ref\_eq}}$$

$$\mathbf{i^s_{ref\_eq}} = G_{vsc}(s)\mathbf{i^s_{ref}} + \frac{\mathbf{v^s_g}}{Z_g(s)} \qquad (7)$$

$$Z_t(s) = \frac{1}{Y_g(s) + Y_{vsc}(s)} = \frac{1/Y_g(s)}{1 + Y_{vsc}(s)/Y_g(s)},$$

and it can be represented by the transfer function

$$F(s) = Z_t(s) = \frac{M(s)}{1 + L(s)} \qquad L(s) = M(s)N(s), \qquad (8)$$

TABLE I. VSC PARAMETERS

Switching frequency	f_{sw}	2.5 kHz
Filter resistance	R_f	0.0075 mΩ
Filter inductance	L_f	0.07 mH
Filter capacitance	C_f	1150 μF
Closed-loop time constant	$\tau_c = 1/\alpha_c$	1 ms
Voltage filter bandwidth	$f_f = \alpha_f/2\pi$	1.25 kHz
PI control proportional gain	$k_p = \alpha_c \cdot L_f$	0.07
PI control integral gain	$k_i = \alpha_c \cdot R_f$	0.0075
Time delay	$T_d = 1.5/f_s$	0.3 ms

where $L(s)$ is the loop transfer function and

$$M(s) = \frac{1}{Y_g(s)} \qquad N(s) = Y_{vsc}(s) \qquad (9)$$

are the open-loop and feedback transfer functions, respectively.

If the outer loops are considered in the VSC characterization, the VSC model in $\alpha\beta$- or dq-frame is a two-dimensional MIMO system because VSC must be represented by real vectors and transfer matrices. The impedance-based representation of the grid-connected VSC system (8) becomes [23],

$$F(s) = [I + L(s)]^{-1} Z_g(s) \qquad L(s) = Y_{vsc}(s)Z_g(s), \qquad (10)$$

where, considering the $\alpha\beta$-frame,

$$
Y_{vsc}(s) = \begin{bmatrix} Y_{vsc\_\alpha\alpha}(s) & Y_{vsc\_\alpha\beta}(s) \\ Y_{vsc\_\beta\alpha}(s) & Y_{vsc\_\beta\beta}(s) \end{bmatrix}
$$

$$
Z_g(s) = \begin{bmatrix} Z_{g\_\alpha\alpha}(s) & 0 \\ 0 & Z_{g\_\beta\beta}(s) \end{bmatrix}
$$

$$ \qquad (11) $$

$$
L(s) = \begin{bmatrix} L_{\alpha\alpha}(s) & L_{\alpha\beta}(s) \\ L_{\beta\alpha}(s) & L_{\beta\beta}(s) \end{bmatrix} =
$$

$$
\begin{bmatrix} Y_{vsc\_\alpha\alpha}(s)Z_{g\_\alpha\alpha}(s) & Y_{vsc\_\alpha\beta}(s)Z_{g\_\beta\beta}(s) \\ Y_{vsc\_\beta\alpha}(s)Z_{g\_\alpha\alpha}(s) & Y_{vsc\_\beta\beta}(s)Z_{g\_\beta\beta}(s) \end{bmatrix}.
$$

III. PASSIVITY AND STABILITY OF GRID-CONNECTED VSCS

Harmonic resonance can destabilize grid-connected VSCs due to VSC non-passivity [4], [13]. These instabilities can be investigated from the impedance-based closed-loop system in Fig. 1(c). This impedance-based system allows stability to be assessed from a frequency-domain approach. Frequency domain methods for stability assessment must analyze the system response for positive- ($s = j\omega$, $\omega > 0$) and negative- ($s = -j\omega$, $\omega > 0$) sequence because the frequency response of $F(j\omega)$ and $F(-j\omega)$, $\omega > 0$ may not be equal since $F^*(j\omega)$ may be different from $F(-j\omega)$ (see example in Appendix A) [11], [23]. Passivity and stability analysis can be considered in the study.

A. Passivity

According to [13], the closed-loop system defined by $F(s)$ in (8) is passive if $M(s)$ and $N(s)$ are passive (i.e., $M(s)$ and $N(s)$ are stable, $\text{Re}\{M(j\omega)\} \geq 0$, $-\infty < \omega < \infty$, and $\text{Re}\{N(j\omega)\} \geq 0$, $-\infty < \omega < \infty$) because it is verified that $F(s)$ is also passive, i.e.,
- $F(s)$ is stable since $-\pi \leq \arg\{L(j\omega)\} \leq \pi$, $-\infty < \omega < \infty$, and therefore the Nyquist criterion is satisfied.
- $\text{Re}\{F(j\omega)\} \geq 0$, $\forall \omega$.

B. Stability

The passivity condition of grid-connected VSC systems can be reduced when only their stability is analyzed because $F(s)$

in (8) is not necessarily unstable if $M(s)$ and $N(s)$ are not passive. For these cases, system stability can be studied in different ways:
- Analyzing the state-space eigenvalues, the poles of $F(s)$ or the roots of $1 + L(s) = Y_g(s) + Y_{vsc}(s) = 0$.
- Applying the Nyquist criterion to the loop transfer function $L(s)$ for $s = j\omega$, $-\infty < \omega < \infty$ or the phase and gain margin conditions from the Bode diagram to the loop transfer function $L(s)$ for $s = \pm j\omega$, $\omega > 0$ [9] − [13], [21].
- Applying the impedance-based stability criterion. This criterion evaluates the difference between the phase of the VSC and grid admittances $Y_{vsc}(\pm j\omega)$, $Y_g(\pm j\omega)$, $\omega > 0$ at frequencies where their magnitudes intersect [10] − [12].
- Applying the positive-net-damping stability criterion in [19], [20] or the alternative approach to this criterion presented in the paper. These criteria evaluate the net damping contribution of grid and VSC admittances at resonance frequencies (see next Section).

The impedance-based and positive-net-damping stability criteria allow analyzing stability considering the contribution of each system admittance.

IV. POSITIVE-NET-DAMPING STABILITY CRITERION

The positive-net-damping stability criterion is proposed and strictly demonstrated for stability studies of SISO systems in [18] − [20]. It is applied to subsynchronous torsional interactions in [18] and two-terminal VSC-HVDC systems in [20]. Although this criterion is a powerful tool for stability assessment, it does not characterize the frequency of the closed-loop unstable oscillatory modes. A reformulation of the positive-net-damping stability criterion for harmonic resonance instabilities of SISO feedback systems is presented to address the above drawback. This is analytically demonstrated in the frequency- and s-domains.

A. Study in the frequency-domain

Considering that $M(s)$ and $N(s)$ are both stable, the closed-loop system defined by $F(s)$ in (8) is asymptotically stable if the Nyquist curve of the loop transfer function $L(s) = M(s)N(s)$ for $s = j\omega$, $-\infty < \omega < \infty$ does not encircle the −1 point. In the literature, the analysis of the Nyquist criterion is conducted from the gain margin condition to prove the positive-net-damping stability criterion for SISO feedback systems [19]. The alternative approach of the positive-net-damping stability criterion in the paper is based on the impedance-based stability criterion [10] − [12] which evaluates the phase margin condition of the Nyquist criterion. In the following Subsections, the study of the positive-net-damping stability criterion based on the gain and phase margin conditions are presented. Although these criteria must be evaluated for the positive- ($s = j\omega$, $\omega > 0$) and negative- ($s = -j\omega$, $\omega > 0$) sequence [11], [12], [23], the study below is made considering only the positive sequence for sake of simplicity in the exposition. Nevertheless, the conclusions must also be applied for the negative-sequence.

This article has been accepted for publication in a future issue of this journal, but has not been fully edited. Content may change prior to final publication. Citation information: DOI 10.1109/JESTPE.2017.2707533, IEEE Journal of Emerging and Selected Topics in Power Electronics

5

1) Positive-net-damping criterion from the gain margin

The analysis of the Nyquist criterion from the gain margin means that $L(s)$ must verify two necessary conditions at the same angular frequency ω:

$$\text{Im}\{M(j\omega)N(j\omega)\} = 0, \tag{12}$$

$$M(j\omega)N(j\omega) > -1. \tag{13}$$

Note that the $M(j\omega)N(j\omega)$ value at the frequency of (12) is the cross point of the Nyquist curve $L(j\omega)$ with the real axis which should be on the right hand side of -1 to ensure stability, i.e. (13) may be hold. The above conditions lead to the theorem proposed in [19], which states that the closed-loop system $F(s)$ in (8) is asymptotically stable if the net damping of the system is positive, i.e., $\text{Re}\{Y_g(j\omega) + Y_{vsc}(j\omega)\} > 0$, at the angular frequencies for which $\text{Im}\{M(j\omega)N(j\omega)\} = 0$ (i.e., at the angular frequencies where the Nyquist curve intersects with the real axis). This theorem allows system stability to be accurately evaluated. The positive-net-damping stability criterion is derived from the above theorem to avoid solving (12). This criterion states that the closed-loop system is asymptotically stable if the net damping of the system is positive for low frequencies where $|M(j\omega)N(j\omega)| > 1$, as well as in the neighborhood of each open-loop $M(j\omega)$ and $N(j\omega)$ resonance (i.e., in the neighborhood of the grid and VSC resonances). The conditions that replace the equation of the Nyquist curve intersection with the real axis in (12) are based on [18] and provide reasonable possibilities of stability for SISO feedback systems. However, they do not provide a clear relation between harmonic resonances of the grid-connected VSC system and stability (see Section V). The application of this criterion is not limited to an impedance-based representation of the grid and VSC as presented in [20].

2) Positive-net-damping criterion from the phase margin

The analysis of the Nyquist criterion from the phase margin means that $L(j\omega)$ must verify the following two necessary conditions at the same angular frequency ω [9] − [11]:

$$|M(j\omega)N(j\omega)| = 1, \tag{14}$$

$$-\pi \le \arg\{M(j\omega)N(j\omega)\} \le \pi. \tag{15}$$

Considering the frequency response of the positive-sequence grid and the VSC admittances in Fig. 1(b) as follows:

$$Y_g(j\omega) = \frac{1}{Z_g(j\omega)} = G_g(\omega) + jB_g(\omega)$$

$$Y_{vsc}(j\omega) = G_{vsc}(\omega) + jB_{vsc}(\omega), \tag{16}$$

the loop transfer function $L(s) = M(s)N(s)$ can be written as the following expression:

$$L(j\omega) = M(j\omega)N(j\omega) = \frac{G_{vsc}(\omega) + jB_{vsc}(\omega)}{G_g(\omega) + jB_g(\omega)}, \tag{17}$$

which combines the stability conditions with the admittances of the equivalent circuit in Fig. 1(b).

The first phase margin condition (14) can be expressed as

$$|L(j\omega)| = \frac{|Y_{vsc}(j\omega)|}{|Y_g(j\omega)|} = \frac{\sqrt{G_{vsc}^2(\omega) + B_{vsc}^2(\omega)}}{\sqrt{G_g^2(\omega) + B_g^2(\omega)}} = 1 \tag{18}$$

$$\Rightarrow \quad G_g^2(\omega) + B_g^2(\omega) = G_{vsc}^2(\omega) + B_{vsc}^2(\omega).$$

Considering the main reactive (inductive or capacitive) nature of the grid and VSCs at harmonic resonances (see Section II), $G_i(\omega) << B_i(\omega)$ for $i = g, vsc$ and (18) can be approximated as

$$B_g(\omega) \approx \pm B_{vsc}(\omega). \tag{19}$$

The parallel resonance observed from the VSC current source in Fig. 1(b) considering the main capacitive and inductive nature of the grid and VSCs at the harmonic resonances (i.e., considering that $G_i(\omega) << B_i(\omega)$ $i = g, vsc$), can be expressed as

$$\text{Im}\{Y_g(j\omega) + Y_{vsc}(j\omega)\} \approx 0 \quad \Rightarrow \quad B_g(\omega) \approx -B_{vsc}(\omega), \tag{20}$$

which matches with the negative sign expression in (19). Thus, this parallel resonance is a particular case of the stability condition $|M(j\omega)N(j\omega)| = 1$. The parallel resonance can also be obtained from the parallel equivalent impedance $Z_t(j\omega)$ (7). Most resonance studies in grid-connected VSC systems consider VSC as an ideal current source and impose $B_g(\omega) = 0$ to characterize parallel resonance [3]. However, Section VI shows that this approximation can provide inaccurate results.

The second phase margin condition (15) can be expressed in terms of the imaginary part of $M(j\omega)N(j\omega)$ in the following two cases

- Case #1: If $d|L(j\omega)|/d\omega > 0$,

$$0 < \arg\{L(j\omega)\} < \pi : G_g(\omega)B_{vsc}(\omega) - G_{vsc}(\omega)B_g(\omega) > 0. \tag{21}$$

- Case #2: If $d|L(j\omega)|/d\omega < 0$,

$$-\pi < \arg\{L(j\omega)\} < 0 : G_g(\omega)B_{vsc}(\omega) - G_{vsc}(\omega)B_g(\omega) < 0. \tag{22}$$

Imposing the parallel resonance relation (20), (21) and (22) can be rewritten as

Case #1:
$$d|L(j\omega)|/d\omega > 0 \quad \Rightarrow \quad B_{vsc}(\omega)\big(G_g(\omega) + G_{vsc}(\omega)\big) > 0$$

Case #2:
$$d|L(j\omega)|/d\omega < 0 \quad \Rightarrow \quad B_{vsc}(\omega)\big(G_g(\omega) + G_{vsc}(\omega)\big) < 0. \tag{23}$$

As demonstrated in Appendix B, Case #1 is produced by inductive grid and capacitive VSC admittances (i.e., $B_g < 0$ and $B_{vsc} > 0$, respectively) and Case #2 is produced by capacitive grid and inductive VSC admittances (i.e., $B_g > 0$ and $B_{vsc} < 0$, respectively). Therefore, the condition in (23) is always satisfied if

$$G(\omega) = G_g(\omega) + G_{vsc}(\omega) > 0, \tag{24}$$

where the conductance $G(\omega)$ corresponds to the net damping of the grid-connected VSC, the conductance $G_g(\omega)$ is the grid damping and the conductance $G_{vsc}(\omega)$ is the VSC damping. Therefore, grid-connected VSC systems are asymptotically stable if (24) holds at the angular frequency ω for which (20) holds. This result demonstrates an alternative approach for the positive-net-damping stability criterion based on the gain margin condition [19]: grid-connected VSC systems are asymptotically stable if net damping $G(\omega)$ is positive in a neighborhood of parallel resonances between the grid and VSC admittances. This demonstration can be extended to SISO feedback systems derived from impedance-based equivalent circuits if the equivalent resistances of the circuit are not significant compared to the reactances (i.e., the equivalent impedances of the circuit are mainly inductive or capacitive). Although the criterion is demonstrated for the positive-sequence ($s = j\omega$, $\omega > 0$), it must also applied for the negative-sequence ($s = -j\omega$, $\omega > 0$). Note that, although the VSC could be considered as an ideal current source for parallel resonance determination, its representation as a Norton equivalent source is necessary to consider the VSC control influence on net damping, and therefore on electrical resonance instabilities. If the VSC is connected to a passive grid, grid damping $G_g(\omega)$ is always positive and the converter control could be designed only by considering the passivity conditions of the VSC equivalent admittance [4], [13], [14].

If the outer loops are considered in the VSC characterization, the VSC model in $\alpha\beta$- or dq-frame is a two-dimensional MIMO system (10) and the stability must be analyzed using the generalized Nyquist criterion (GNC) which extends the traditional Nyquist criterion to the eigenloci of the system return-ratio matrix (i.e., to the Nyquist curves of the eigenvalues of the loop gain transfer matrix) [9], [23]. These eigenvalues are obtained from the loop transfer function $L(s)$ (11),

$$\det[\lambda_i(s)I - L(s)] = 0 \qquad (i = 1, 2) \;\Rightarrow\; \lambda_{1,2}(s) =$$

$$\frac{L_{\alpha\alpha}(s) + L_{\beta\beta}(s)}{2} \pm \sqrt{\left(\frac{L_{\alpha\alpha}(s) - L_{\beta\beta}(s)}{2}\right)^2 + L_{\alpha\beta}(s)L_{\beta\alpha}(s)}. \tag{25}$$

The non-diagonal terms of the VSC transfer matrix function (11) are usually smaller than the diagonal terms [9], and therefore the non-diagonal terms of the loop transfer function $L(s)$ can be neglected in front of the diagonal terms. Considering this approximation, the eigenvalues of the loop transfer function result as

$$\lambda_{1,2}(s) = \frac{L_{\alpha\alpha}(s) + L_{\beta\beta}(s)}{2} \pm \frac{L_{\alpha\alpha}(s) - L_{\beta\beta}(s)}{2}$$

$$\Rightarrow \begin{cases} \lambda_1(s) = L_{\alpha\alpha}(s) = Y_{vsc\_\alpha\alpha}(s)Z_{g\_\alpha\alpha}(s) \\ \lambda_2(s) = L_{\beta\beta}(s) = Y_{vsc\_\beta\beta}(s)Z_{g\_\beta\beta}(s). \end{cases} \tag{26}$$

In this case, the impedance-based and positive-net-damping stability criteria may be directly applied to the $\alpha\alpha$- and $\beta\beta$-components for stability assessment. Otherwise, there is not

obvious relation between the GNC and the impedance-based and positive-net-damping stability criteria and further analysis (out of the paper scope) should be made to extend the application of these criteria to MIMO systems. The above comments can also be applied to dq-frame.

B. Study in the s-domain

The positive-net-damping stability criterion applied for harmonic resonance instabilities can also be demonstrated by analyzing the poles of $F(s)$ or the roots of $1 + L(s) = 0$ in (8). Considering that the dominant pole of the system is the poorly-damped pole related to the harmonic parallel resonance between the grid and the VSC [20] and that around this resonance the VSC has an inductive response and the grid has a capacitive response (see Section II and example in Section VI), the grid and VSC admittances in (9) can be expressed as follows:

$$Y_g(s) \approx \frac{1}{R_g + 1/(C_g s)} \qquad Y_{vsc}(s) \approx \frac{1}{R_{vsc} + L_{vsc}s}, \tag{27}$$

and the positive-sequence equivalent admittance observed form the VSC current source in Fig. 1(b) is

$$Y_g(j\omega) + Y_{vsc}(j\omega) \approx \frac{1}{R_g - j/(C_g\omega)} + \frac{1}{R_{vsc} + jL_{vsc}\omega}$$

$$= \frac{R_g + j/(C_g\omega)}{R_g^2 + 1/(C_g\omega)^2} + \frac{R_{vsc} - jL_{vsc}\omega}{R_{vsc}^2 + (L_{vsc}\omega)^2}. \tag{28}$$

The terms R_g^2 and R_{vsc}^2 can be neglected with respect to the terms $1/(C_g\omega)^2$ and $(L_{vsc}\omega)^2$ due to the main capacitive and inductive response of the grid and VSCs. Thus, the equivalent admittance can be approximated as

$$Y_g(j\omega) + Y_{vsc}(j\omega)$$

$$\approx R_g(C_g\omega)^2 + \frac{R_{vsc}}{(L_{vsc}\omega)^2} + j\left(C_g\omega - \frac{1}{L_{vsc}\omega}\right). \tag{29}$$

Moreover, considering (27), $1 + L(s)$ can be written as

$$1 + L(s) = 1 + \frac{R_g + 1/(C_g s)}{R_{vsc} + L_{vsc}s} = \frac{C_g L_{vsc}s^2 + C_g(R_g + R_{vsc})s + 1}{C_g s(R_{vsc} + L_{vsc}s)}. \tag{30}$$

The roots of (30) are

$$s = \frac{-C_g(R_g + R_{vsc}) \pm \sqrt{C_g^2(R_g + R_{vsc})^2 - 4C_g L_{vsc}}}{2C_g L_{vsc}}, \tag{31}$$

which, considering that $C_g(R_g + R_{vsc})^2 << 4L_{vsc}$, can be approximated as

$$s \approx -\frac{R_g + R_{vsc}}{2L_{vsc}} \pm j\frac{1}{\sqrt{C_g L_{vsc}}}. \tag{32}$$

It can be observed that the parallel resonance condition in (29) matches with the imaginary part of the roots in (32).
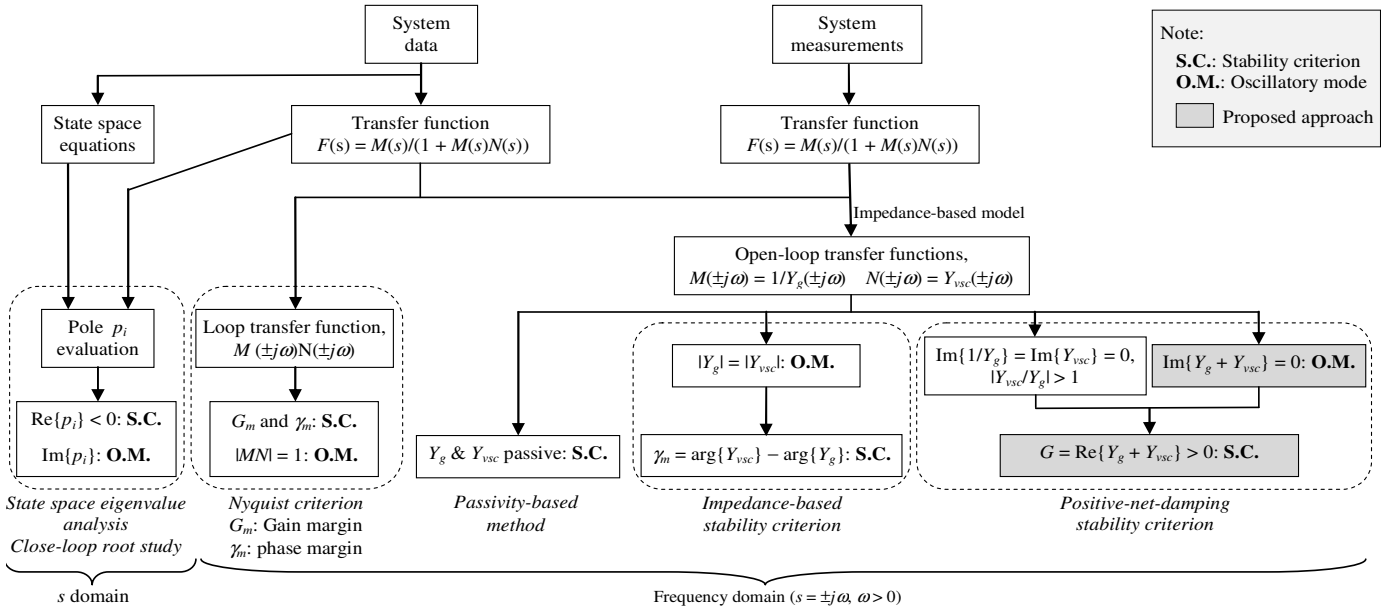
Fig. 3. Flowcharts of stability methods in grid-connected VSC systems.

Moreover, according to (29), if (24) holds (i.e., if (29) is passive) at the resonance frequency, the poles have a negative real part:

$$G_g(\omega) + G_{vsc}(\omega) = \frac{R_g + R_{vsc}}{(L_{vsc}\omega)^2} > 0 \quad \Rightarrow \quad -\frac{R_g + R_{vsc}}{2L_{vsc}} < 0. \quad (33)$$

From this demonstration, it can be stated that the frequency at the parallel resonance observed from the VSC current source approximately matches with the frequency of the oscillations in case of instability. Thus, the alternative approach of the positive-net-damping stability criterion based on the phase margin condition allows predicting the frequency of the closed-loop unstable oscillatory modes. It can be observed in (32) that a negative VSC resistance R_{vsc} may lead to a positive real part of the poles if $|R_{vsc}| > |R_g|$ (i.e., to a system instability) which is correctly predicted with the negative value of the net damping $G_g(\omega) + G_{vsc}(\omega)$ in (33).

V. COMPARISON OF STABILITY METHODS

Fig. 3 shows the flowchart of the different methods for stability assessment of grid-connected VSC systems and Table II presents their main characteristics. The state space eigenvalue analysis (or closed-loop root study) is a useful tool to analyze the impact of system and control parameters on stability [8]. However, this method requires detailed information for all elements in the system (including physical and control parameters) and high-order dynamic models for large systems that could exceed the computation limits of the solvers due to the large amount of information to manage from these models which must be update every time if any of the system parameter changes. Moreover, this information is not always completely available limiting an adequate system modeling. On the other hand, frequency domain methods are used to identify the causes of instabilities with less compute-intensive effort and less detailed system information [9] – [20]. These methods can be applied by using either simulations or system measurements if the system parameter information of analytical models is not available, which offers an advantage over the state space eigenvalue analysis.

The Nyquist criterion and the Bode diagram are the most used frequency domain methods but these methods only show numerical results and they focus on the loop transfer function of the entire system which does not allow investigating separately the contribution of the source and load subsystems to the closed-loop stability [9] – [13]. This may limit the analysis of oscillations and instabilities caused by particular impedances or filters connected to the system even though the loop transfer function could be measured. These drawbacks are avoided with the frequency domain methods that analyze the individual contribution of the source and load subsystems from the open-loop transfer functions [4], [9] – [20]. Among these methods, the passivity-based method imposes passivity in each subsystem (i.e., $G_g(\omega) > 0$ and $G_{vsc}(\omega) > 0$, (16)) in order to ensure the closed-loop system stability [4], [13], [14], while the impedance-based and the positive-net-damping stability criteria are less restrictive and do not impose this passivity condition because consider the contribution of each subsystem to stability assessment. As an example, the positive-net-damping stability criterion ensures the closed-loop system stability if $G_g(\omega) + G_{vsc}(\omega) > 0$ (24), and therefore a system could be stable even when the VSCs are not passive (i.e., even with $G_{vsc}(\omega) < 0$) if $G_g(\omega) > 0$ and $|G_g(\omega)| > |G_{vsc}(\omega)|$. For all the previous comments, the impedance-based stability criterion [10] – [12] and the positive-net damping stability criterion based on the gain [19], [20] or phase margin conditions are useful tools for stability analysis offering several advantages in front of the other methods. Based on Fig. 3 and Table II, a comparison between the impedance-based and the positive-net-damping stability criteria is presented below.

TABLE II. CHARACTERISTICS OF METHODS FOR STABILITY ASSESSMENT

		State space analysis	Nyquist criterion	Passivity method	Impedance-based criterion	Positive-net-damping criterion	New approach
System data requirements	Detailed information	✓	✓	✓	✓	✓	✓
	Measurements	✗	✓	✓	✓	✓	✓
Evaluation of the method	Simple to evaluate	✗	✓	✓	✓	✓	✓
	Short computation effort	✗	✓	✓	✓	✓	✓
	Subsystem contribution to stability	✓	✗	✗	✓	✓	✓
	Oscillatory mode information	✓	✓	✗	✓	✗	✓
	Criterion based on system resistances	✗	✗	✓	✗	✓	✓
Stability analysis	Identification of instability causes	✓	✓	✓	✓	✓	✓
	Physical interpretation of instabilities	✓	✗	✗	✗	✗	✓

According to (18), (19) and (20) and considering that the grid-connected VSC system resistances are smaller than the reactances, the condition $|Y_g(j\omega)| = |Y_{vsc}(j\omega)|$ (i.e., the intersection of the grid and VSC admittances) of the impedance-based stability criterion is equivalent to the condition of the proposed positive-net-damping stability criterion $\text{Im}\{Y_g(j\omega) + Y_{vsc}(j\omega)\} = 0$ (i.e., the parallel resonances between the grid and VSC admittances) and both conditions provide the frequency of the oscillatory modes (see Subsection IV.B). Subsequently, the phase angle between the VSC and the grid admittance ratio (i.e., the phase margin of the loop transfer function, $\gamma_m = \arg\{Y_{vsc}(j\omega)\} - \arg\{Y_g(j\omega)\}$) in the impedance-based stability criterion and the net damping $G(\omega) = G_g(\omega) + G_{vsc}(\omega)$ (24) in the proposed positive-net-damping stability criterion are evaluated at the above frequency to analyze stability. The evaluation of the damping stability condition $G_g(\omega) + G_{vsc}(\omega) > 0$ is more practical than the evaluation of the phase margin condition $\gamma_m = \arg\{Y_{vsc}(j\omega)\} - \arg\{Y_g(j\omega)\}$ because damping is directly related to system resistances which are a common parameter in electric power systems (negative or small values of system resistances at specific frequencies may lead to instability problems). Moreover, the damping can be analytically characterized with simpler expressions than the phase margin because it is easier handle mathematically the real part of the source and load impedance sum than the phase angle of the source and load impedance ratio. As an example, let assume that the grid is modeled as a capacitor C_g in parallel with the short-circuit resistance R_g and inductance L_g, and the VSC model (6) is determined neglecting the filter resistance (i.e., $R_f = 0$ and $k_i = \alpha_c \cdot R_f = 0$) and considering that $|\omega| \gg \{\omega_1, \alpha_f\}$ at the analyzed frequencies [14]. The positive-sequence grid and VSC admittances can be written as

$$Y_g(j\omega) = jC_g\omega + \frac{R_g - jL_g\omega}{R_g^2 + L_g^2\omega^2}$$

$$Y_{vsc}(j\omega) \approx$$
$$\frac{1}{L_f(j\omega + \alpha_c e^{-j\omega T_d})} = \frac{\alpha_c \cos(\omega T_d)}{L_f(\omega^2 + \alpha_c^2 - 2\alpha_c\omega\sin(\omega T_d))} + \quad (34)$$
$$j\frac{\alpha_c \sin(\omega T_d) - \omega}{L_f(\omega^2 + \alpha_c^2 - 2\alpha_c\omega\sin(\omega T_d))},$$

and the stability conditions of the proposed positive-net-damping stability criterion at the grid and VSC parallel resonances become

$$G_g(\omega) + G_{vsc}(\omega) =$$
$$\frac{R_g}{R_g^2 + L_g^2\omega^2} + \frac{\alpha_c \cos(\omega T_d)}{L_f(\omega^2 + \alpha_c^2 - 2\alpha_c\omega\sin(\omega T_d))} > 0, \quad (35)$$

which is much easier to analytically handle and to physically relate with the system resistances that the stability condition of the impedance-based stability criterion because the phase of $Y_{vsc}(j\omega)\}$ and $Y_g(j\omega)$ is complicated to determine analytically. Another example can be found in [22], where the influence of different VSC parameters is graphically analyzed from the VSC damping evaluated with the phase of the VSC transfer function but this study could be performed analytically if the VSC damping was evaluated with the real part of the VSC transfer function.

The positive-net-damping stability criterion based on the gain margin condition evaluates the net damping at the frequencies derived from the conditions $\text{Im}\{1/Y_g(j\omega)\} \approx 0$, $\text{Im}\{Y_{vsc}(j\omega)\} \approx 0$ and $|Y_{vsc}(j\omega)/Y_g(j\omega)| > 1$ (i.e., at the frequencies of the open-loop resonances and the loop gain greater than 1). Considering (16), these conditions can be

expressed as

$$\text{Im}\left\{\frac{1}{Y_g(j\omega)}\right\} \approx 0 \quad \Rightarrow \quad B_g(\omega) \approx 0$$

$$\text{Im}\left\{Y_{vsc}(j\omega)\right\} \approx 0 \quad \Rightarrow \quad B_{vsc}(\omega) \approx 0$$

$$\left|\frac{Y_{vsc}(j\omega)}{Y_g(j\omega)}\right| = \frac{\sqrt{G_{vsc}^2(\omega)+B_{vsc}^2(\omega)}}{\sqrt{G_g^2(\omega)+B_g^2(\omega)}} > 1 \quad \Rightarrow \qquad (36)$$

$$G_g^2(\omega)+B_g^2(\omega) > G_{vsc}^2(\omega)+B_{vsc}^2(\omega) \quad \Rightarrow$$

$$\left|B_g(\omega)\right| \succ \left|B_{vsc}(\omega)\right|.$$

which match neither with the first gain margin condition (12)

$$\text{Im}\left\{M(j\omega)N(j\omega)\right\} = \text{Im}\left\{\frac{G_{vsc}(\omega)+jB_{vsc}(\omega)}{G_g(\omega)+jB_g(\omega)}\right\} = 0 \quad \Rightarrow$$
$$\qquad\qquad\qquad\qquad\qquad\qquad\qquad\qquad\qquad\qquad (37)$$
$$G_g(\omega)B_{vsc}(\omega)-G_{vsc}(\omega)B_g(\omega) = 0,$$

nor with the first phase margin condition (19). Therefore, the frequencies obtained from (36) should not be strictly applied in the second gain and phase margin conditions (13) and (15) to derive the positive-net-damping stability criterion. Moreover, according to (19), the frequency of the oscillatory modes are not characterized by the conditions $B_g(\omega) \approx 0$ and $B_{vsc}(\omega) \approx 0$ in (36) and it may only be contained in the frequency range defined by $|B_g(\omega)| \succ |B_{vsc}(\omega)|$. This frequency range could be wide depending on the grid-connected VSC system [20]. As alternative, the proposed positive-net-damping stability criterion uses the frequency of the parallel resonances between the grid and VSC admittances. This parallel resonance condition is directly derived from (14), it is easy to determine from the impedance-based characterization of the system and approximately provides the frequencies of the oscillatory modes.

According to the previous comparison, the positive-net-damping stability criterion proposed in the paper offers several advantages respect to the impedance-based and positive-net-damping stability criteria because it collects the best of them, i.e., the evaluation of the net damping, which is more practical than the phase angle between the VSC and the grid admittance ratio, and the evaluation of the parallel resonances between the grid and VSC admittances, which provides specific frequencies related with the oscillatory modes and it is easy to characterize. A recent work in [21] investigates near-synchronous resonance instabilities in grid-connected VSC systems and the impact of PLL on the near-synchronous grid-connected VSC oscillations from the damping at the frequency of the closed-loop oscillatory modes (called as intrinsic oscillatory points). The intrinsic oscillatory points are found from a VSC model which only considers the PI controller. This model leads to a system equivalent impedance with a constant resistance (i.e., the equivalent resistance does not depend on the frequency) and the resonance condition can be directly applied to the imaginary part of the impedance without neglecting the resistance (20). The stability criterion is established from the net damping analysis of the system's transfer function at the intrinsic oscillatory points obtained with the simplified VSC model. This procedure results from the application of the complex torque coefficients method which is presented, but not strictly proof, to study subsynchronous torsional interactions of turbine-generator sets [15], [16]. This method is also used and mathematically analyzed in [17] and [18] presenting some cases where it does not correctly predict closed-loop oscillatory modes and instabilities of torsional interactions. The application of the proposed approach is similar to the complex torque coefficients method but it is mathematically demonstrated and extends its application to assess harmonic resonance instabilities in SISO feedback systems and MIMO feedback systems with negligible non-diagonal terms of the loop transfer function (e.g., grid-connected VSC systems). According to the proposed approach, the oscillatory modes are obtained from the parallel resonance between the grid and VSC admittances considering all the system and control parameters of the models. In this case, the resistance of the system's equivalent
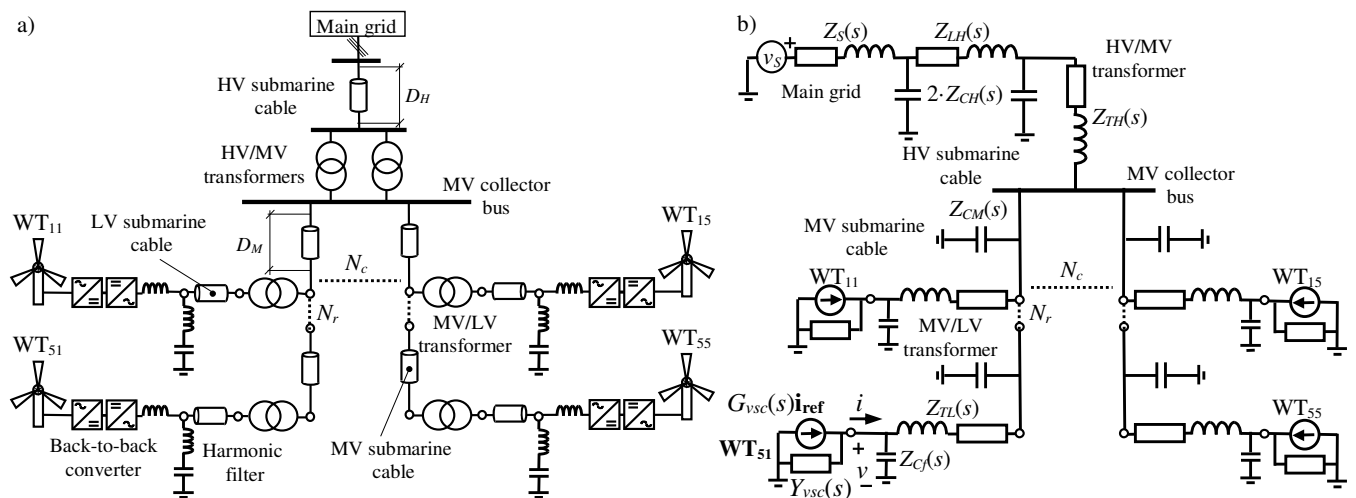

Fig. 4. Offshore WPP system: a) WPP connection scheme. b) Single-line equivalent circuit.

impedance may depend on frequency, and the resonance condition can only be applied if resistances are smaller than reactances.

VI. APPLICATION

The application of the different methods to study harmonic resonance instabilities is illustrated in an offshore WPP. The alternative approach of the positive-net-damping stability criterion is compared with the other methods. This application is an example of a grid with multiple VSCs. The connection of multiple VSCs may affect the frequency response of the grid changing the frequency range of its capacitive response (i.e., changing the frequency of the parallel resonances) and it may also affect the damping of the grid because the non-passive response of the connected VSCs at the studied frequencies may reduce the grid damping and worsen system stability. However, the above influence does not affect the application of the different approaches and the assumptions of these approaches as it can be verified in the next Subsections.

A. Description

A 125 MW offshore WPP with 25 type-4 WTs (i.e., full-scale VSC WTs) is studied according to Fig. 4(a). The WPP consists of five 5-WT strings (i.e., $N_r = 5$ and $N_c = 5$). The WTs are connected at 0.69 kV, which is stepped up to 33 kV for the collector system and to 150 kV for the export system with a group of two 125 MVA transformers in parallel. Type-4 WTs are equipped with two converters in back-to-back and harmonic filters are usually installed on the grid side of WT converters to mitigate frequency switching harmonics. Data of the VSC control and the WPP are shown in Table I and Table III, respectively. Instability problems can arise due to the interaction between the grid side VSC control of WTs and the WPP [7]. In order to analyze these problems, the WT VSC and the control are modeled as a Norton equivalent circuit (5) and the offshore WPP is modeled with the equivalent circuit in

TABLE III. 125 MW OFFSHORE WIND POWER PLANT PARAMETERS

Main grid	Open-circuit voltage	U_o	150 kV (50 Hz)
	Short-circuit power	S_s	10000 MVA
	Ratio X_S/R_S	$\tan\varphi_S$	25
HV/MV transformers	Transformer ratio	U_{NH}/U_{NM}	150/33 kV
	Rated power	S_N	125 MVA
	Short-circuit impedance	ε_{cc}	0.1 pu
	Ratio X_T/R_T	$\tan\varphi_T$	25
HV submarine cable	Longitudinal π resistance	R_L	0.32 Ω/km
	Longitudinal π reactance	X_L	0.126 Ω/km
	Transversal π reactance	X_C	$0.15\cdot10^5$ Ω·km
	Length	D_H	10 km
MV submarine cable	Transversal π reactance	X_C	$0.14\cdot10^5$ Ω·km
	Length	D_M	1 km
MV/LV transformer	Transformer ratio	U_{NM}/U_{NL}	33/0.69 kV
	Rated power	S_N	5 MVA
	Short-circuit impedance	ε_{cc}	0.05 pu
	Ratio X_T/R_T	$\tan\varphi_T$	25
WT	Active power consumption	P_L	5 MW
	Displacement power factor	λ_L	≈ 1.0

Fig. 4(b). In the examples, the HV and MV submarine cables are characterized as single concentrated parameter π circuits because they are short enough to be well represented for low frequencies. Moreover, the MV submarine cable model is simplified as the transversal capacitors of the cable because the longitudinal impedance is not significant compared with the inductance of the transformers. On the other hand, the LV submarine cables are omitted because their capacitance is very small and their longitudinal impedance can be included in the impedance of the MV/LV transformers. The Norton equivalent model (5) and the filter capacitance of the WTs are considered in the study.

WPP stability is analyzed from WT_{51} (see Fig. 4(b)). In order to do that, the VSC WT equivalent admittance $Y_{vsc}(s)$ and the offshore WPP equivalent admittance $Y_g(s)$ observed from the analyzed WT must be determined to perform the stability studies. The former is obtained from (6) and the latter is calculated as follows:

$$Y_g(s) = \frac{Z_{Cf}(s) + Z_{TL}(s) + \dfrac{Z_{e1}(s)Z_{CM}(s)}{Z_{e1}(s) + Z_{CM}(s)}}{Z_{Cf}(s)\left(Z_{TL}(s) + \dfrac{Z_{e1}(s)Z_{CM}(s)}{Z_{e1}(s) + Z_{CM}(s)}\right)}, \qquad (38)$$

where

$$Z_{e1}(s) = \left((N_r N_c - 1)\left(\frac{1}{Z_{CM}(s)} + \frac{1}{Z_{e2}(s)}\right) + \frac{1}{Z_{e3}(s)}\right)^{-1}$$

$$Z_{e2}(s) = \frac{Z_{Cf}(s)/Y_{vsc}(s)}{Z_{Cf}(s) + 1/Y_{vsc}(s)} + Z_{TL}(s)$$

$$Z_{e3}(s) = \frac{Z_{e4}(s)2Z_{CH}(s)}{Z_{e4}(s) + 2Z_{CH}(s)} + Z_{TH}(s) \qquad (39)$$

$$Z_{e4}(s) = \frac{Z_S(s)2Z_{CH}(s)}{Z_S(s) + 2Z_{CH}(s)} + Z_{LH}(s).$$

B. Examples

The effect that the VSC control parameters and passive components have on the stability is analyzed. As an example, the influence that the feedforward low-pass filter bandwidth $f_f = \alpha_f/(2\pi)$ (from 1.25 to 2 kHz) and the converter filter
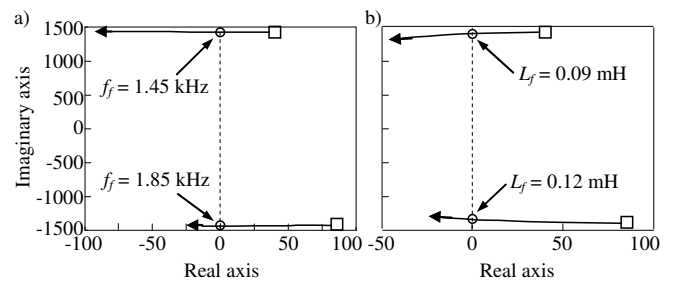
Fig. 5. Root locus of the offshore WPP poles related to the instability: a) Variation of feedforward low-pass filter bandwidth from 1.25 to 2 kHz when $L_f = 0.07$ mH. b) Variation of converter filter inductance from 0.07 to 0.15 mH when $f_f = 1.25$ kHz.

inductance L_f (from 0.07 to 0.15 mH) have on WP stability is studied. The WP stability is analyzed from WT_{51} (see Fig. 4(b)) when the parameters $f_f = \alpha_f/(2\pi)$ and L_f of this WT are modified. Note that the VSC feedforward low-pass filter bandwidth is varied from $\alpha_f = 7.85\alpha_c$ to $\alpha_f = 11.9\alpha_c$ considering the low-pass filter design for transient-mode operation in weak grids. The grid and VSC transfer functions are in phase and dq coordinates, respectively, and they must be in the same frame to evaluate stability. According to Subsection II.B, both transfer functions are transformed to $\alpha\beta$-frame: the VSC transfer function by means of the frequency translation $s \rightarrow s - j\omega_1$ and the grid transfer function is the same as in phase coordinates [23].

The state space eigenvalue analysis (or closed-loop root study) can be used to analyze the impact of system parameters on stability. Multiple poles are numerically obtained from the WPP transfer function and their analysis allows studying the system instabilities. Fig. 5 describes only the root locus of the poles related to instability. These poles are not exactly complex conjugate because the complex gain $jL_f\omega_1$ of the current feedforward in the control law (2) and the transformation of the VSC equivalent admittance from dq coordinates to $\alpha\beta$ coordinates by means of the frequency rotation $s \rightarrow s - j\omega_1$ introduce complex components into the closed-loop transfer function $F(s)$ in (8). These components may produce a different frequency response of $F(j\omega)$ and $F(-j\omega)$, $\omega > 0$ since $F^*(j\omega)$ is different from $F(-j\omega)$ (see

example in Appendix A) [23]. The system becomes unstable when one of the poles moves to the positive side of the real axis, which is equivalent to a negative damping (see Subsection IV.B). As can be seen in Fig. 5, small values of low-pass filter bandwidth may lead to instability problems whereas large values of converter filter inductances may improve resonance stability. It can also be observed that filter bandwidth does not affect closed-loop oscillatory modes while high filter inductance slightly shifts closed-loop oscillatory modes to lower frequencies.

The application of the frequency-domain methods is shown in Fig. 6 and Fig. 7. Only the frequency response of the positive-sequence ($s = j\omega$, $\omega > 0$) is analyzed because it is the first to cause system instability (i.e., it is the less damped). Stable and unstable examples are illustrated modifying the low-pass filter bandwidth ($f_f = 1.9$ and 1.25 kHz, respectively) when $L_f = 0.07$ mH. The Nyquist and Bode diagrams in Fig. 6(a) and Fig. 7(a) confirm the previous results on stability. For $f_f = 1.9$ kHz, the Nyquist curve does not encircle the -1 point (nor the open-loop system has positive poles) and the Bode plot presents a phase margin equal to $\phi_m = 3.3°$. For $f_f = 1.25$ kHz, the Nyquist curve encircles the -1 point in clockwise direction and the Bode plot presents a phase margin equal to $\phi_m = -1.9°$. Note that both methods focus on the loop transfer function $L(s) = M(s) \cdot N(s)$ (8) which does not allow investigating separately the contribution of the subsystems $M(s)$ and $N(s)$ to the closed-loop stability.
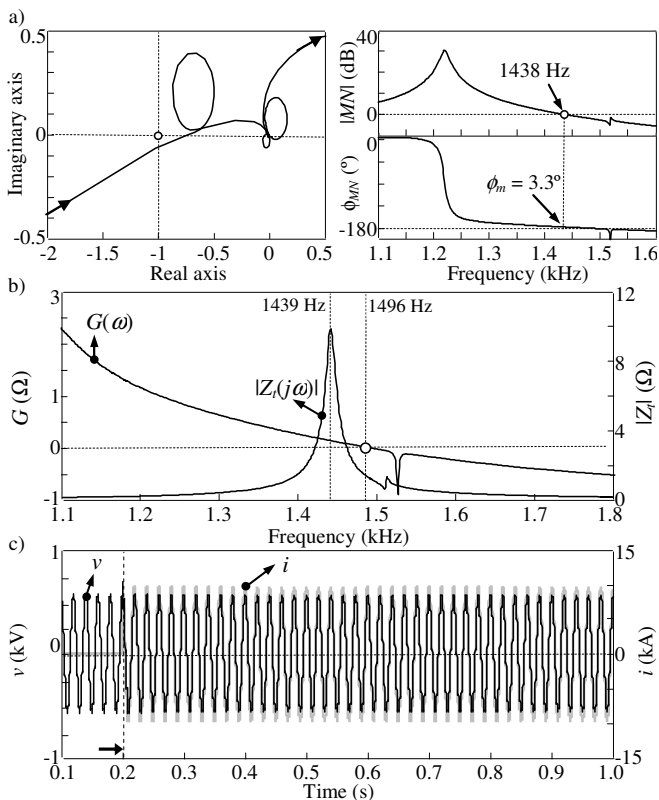

Fig. 6. Stable example of the offshore WPP ($L_f = 0.07$ mH and $f_f = 1.9$ kHz): a) Nyquist (left) and Bode (right) plots of $M(j\omega)N(j\omega)$. b) Frequency response of equivalent impedance and net damping. c) Instantaneous waveforms of the voltage and current at the WT terminals.
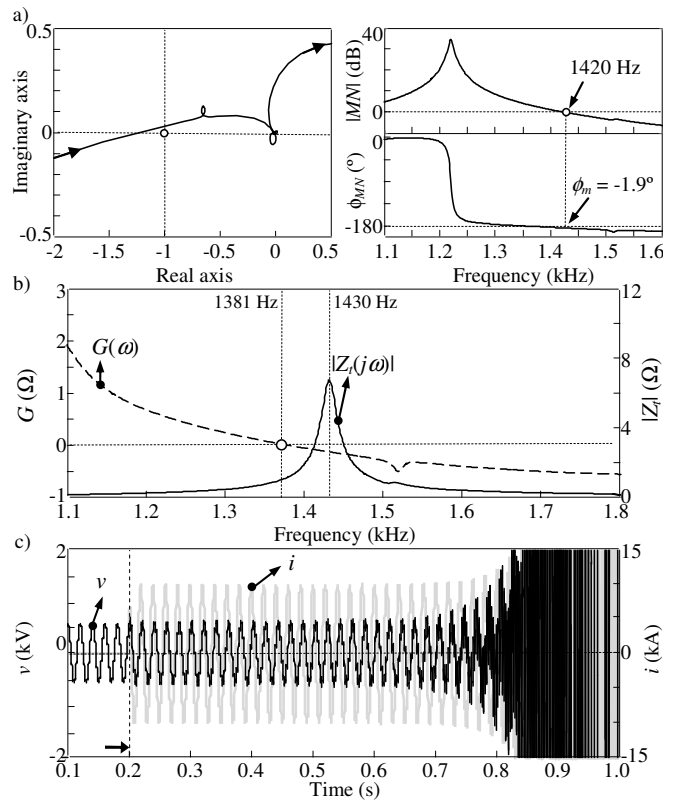
Fig. 7. Unstable example of the offshore WPP ($L_f = 0.07$ mH and $f_f = 1.25$ kHz): a) Nyquist (left) and Bode (right) plots of $M(j\omega)N(j\omega)$. b) Frequency response of equivalent impedance and net damping. c) Instantaneous waveforms of the voltage and current at the WT terminals.
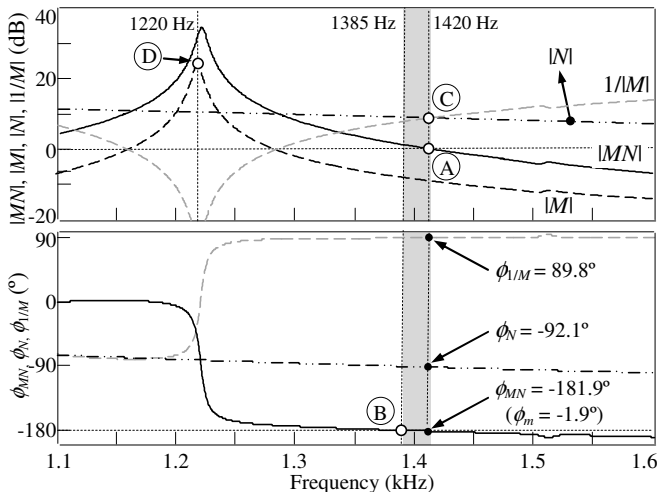
Fig. 8. Comparison of the impedance-based and positive-net-damping stability criteria of the offshore WPP unstable example ($L_f = 0.07$ mH and $f_f = 1.25$ kHz).

The application of the alternative approach of the positive-net-damping stability criterion proposed in the paper is shown in Fig. 6(b) and Fig. 7(b). The frequency response of the equivalent impedance $Z_t(j\omega) = (Y_g(j\omega) + Y_{vsc}(j\omega))^{-1}$ (7) and the net damping $G(\omega)$ shows that the system is stable for $f_f = 1.9$ kHz because the $Z_t(j\omega)$ parallel resonance at 1439 Hz is in the positive damping region. The system becomes unstable when $f_f = 1.25$ kHz due to the negative damping at the $Z_t(j\omega)$ parallel resonance (i.e., at 1430 Hz). These resonances are caused from the interaction between the inductive response of the VSC and the capacitive response of the grid at these frequencies (see Section II). The origin of the instability is a damping reduction in the VSC contribution because the boundary frequency of the negative damping region is decreased from 1496 Hz to 1381 Hz due to the low-pass filter bandwidth decrease [22]. According to the demonstration in Subsection IV.B, the frequency of the resonance matches with the closed-loop oscillatory modes of the poles in Fig. 5. Note that the alternative approach of the positive-net-damping stability criterion combines the advantages of the eigenvalue analysis and Nyquist and Bode criteria: it is simple to evaluate as the Nyquist and Bode criterion and provides information about the cause of instability and the frequency of the oscillatory modes, as the eigenvalue analysis. Moreover, it allows considering the stability contribution of each subsystem. Time-domain simulations in PSCAD/EMTDC are shown in Fig. 6(c) and Fig. 7(c) to validate the stability study. The stable ($f_f = 1.9$ kHz) and unstable ($f_f = 1.25$ kHz) waveforms of the instantaneous voltages and currents at the WT_{51} PCC when this WT is connected at 0.2 s are plotted.

C. Comparison with other frequency-domain methods

The alternative approach of the positive-net-damping stability criterion proposed in the paper is further analyzed in Fig. 8, where the unstable situation in Fig. 7 is represented by plotting the Bode diagram of $N(j\omega) = Y_{vsc}(j\omega)$, $M(j\omega) = 1/Y_g(j\omega)$, $1/M(j\omega)$ and $M(j\omega)N(j\omega)$ (9). According to the demonstration in Subsection IV.A, the $Z_t(j\omega)$ parallel

resonance in Fig. 7 approximately corresponds to the frequency of point A in Fig. 8 where $|M(j\omega)N(j\omega)| = 1$ and the zero crossing point of the net damping $G(\omega)$ in Fig. 7 approximately corresponds to point B in Fig. 8 where $\phi_{MN} = -180°$.

The impedance-based stability criterion [10] − [12] analyzes the system stability from the difference between the phases of $Y_g(j\omega)$ and $Y_{vsc}(j\omega)$ at the frequency of point C. This point corresponds to the intersection of the grid and VSC admittance magnitudes $|Y_g(j\omega)|$ and $|Y_{vsc}(j\omega)|$, and the difference between the phases of $Y_g(j\omega)$ and $Y_{vsc}(j\omega)$ characterizes the phase margin of $M(j\omega)N(j\omega)$, i.e., $\phi_m = 180 − (89.8 − 92.1) = -1.9°$ which identifies the system instability. Comparing the proposed positive-net-damping stability criterion with the impedance-based stability criterion, the stability is evaluated at the same frequency for both methods (i.e., the frequency of the parallel resonance of $Z_t(j\omega)$ at point A and the intersection frequency of $|Y_g(j\omega)|$ and $|Y_{vsc}(j\omega)|$ at point C). Also, the evaluation of the net damping sign is equivalent to determine the phase margin of $M(j\omega)N(j\omega)$ from the difference between the phase of $Y_g(j\omega)$ and $Y_{vsc}(j\omega)$. However, the evaluation of net damping is more practical than the phase evaluation because the resonance instabilities are related to a lack of damping.

The original positive-net-damping stability criterion in [19] analyzes the system stability from the net damping at the open-loop $N(j\omega)$ and $M(j\omega)$ resonances and the frequencies where the loop gain $|M(j\omega)·N(j\omega)|$ exceeds unity. In this case, $N(j\omega)$ does not have any resonance, point D corresponds to the resonance frequency of $M(j\omega)$ and the zone below point A corresponds to the frequency range where $|M(j\omega)·N(j\omega)|$ exceeds unity. The net damping at point D is positive because the phase of $M(j\omega)·N(j\omega)$ is greater than −180°, and therefore the instability is not predicted by the open-loop transfer function $M(j\omega)$. On the other hand, the net damping at frequencies below point A is negative because the phase between points A and B is smaller than −180° (grey area in Fig. 8) which predicts the system instability. It can be noted that in this example the positive-net-damping stability criterion in [19] evaluates the instability of the example from the loop transfer function $M(j\omega)N(j\omega)$ while the proposed positive-net-damping stability criterion evaluates this instability from the grid and the VSC admittance contribution at the resonance of the closed-loop system. Comparing the two positive-net-damping stability criteria, both methods are simple to evaluate, but only the proposed positive-net-damping stability criterion always considers the contribution of each subsystem and provides information of the closed-loop oscillatory mode frequencies.

VII. CONCLUSIONS

This paper proposes an alternative approach of the positive-net-damping stability criterion for assessing harmonic resonance instabilities. The proposed approach demonstrates mathematically the complex torque coefficients method from the evaluation of the phase margin condition at harmonic

resonance frequencies and extends its application to SISO and MIMO feedback systems derived from impedance-based equivalent circuits (e.g., grid-connected VSC systems). This approach can be used if the reactive elements of the system are large compared to the resistive elements (e.g., at the frequencies of the harmonic resonance instabilities in grid-connected VSC systems). The stability criterion proposed in the paper is compared with those in the literature highlighting the following contributions:

- It is simple to evaluate as the frequency domain methods.
- It considers the stability contribution of each subsystem as the impedance-based and positive-net-damping stability criteria.
- It provides an intuitive explanation and physical understanding of the instability phenomenon considering the net damping at electrical resonances as the positive-net-damping criterion.
- It provides a clear relation between harmonic resonances of the grid-connected VSC system and stability.
- It predicts the frequency of unstable oscillations.

APPENDIX A

EXAMPLE OF VSC COMPLEX TRANSFER FUNCTION

An example is presented to illustrate the different response of the VSC complex transfer function for the positive- and negative-sequences.

Assuming $R_f \approx 0$, $k_i = \alpha_c \cdot R_f \approx 0$, $H(s) \approx 1$ (i.e., the low-filter bandwidth is high to decouple VSC and grid dynamics [2]) and approximating the VSC time delay T_d by a first-order transfer function [22] as

$$\mathbf{v_o} \approx \frac{1}{T_d s + 1} \mathbf{v_{ref}}, \quad (40)$$

The VSC equivalent admittance (6) can be written in dq-frame as follows,

$$Y_{vsc}(s) = \frac{T_d s}{L_f \left(T_d s^2 + (1 + j T_d \omega_1) s + \alpha_c \right)}, \quad (41)$$

and the poles of the admittance are

$$T_d s^2 + (1 + j T_d \omega_1) s + \alpha_c = 0$$

$$\Rightarrow \begin{cases} s_1 = -\dfrac{1}{2 T_d} + \kappa_r + j \left(\kappa_i - \dfrac{\omega_1}{2} \right) \\ s_2 = -\dfrac{1}{2 T_d} - \kappa_r - j \left(\kappa_i + \dfrac{\omega_1}{2} \right) \end{cases}, \quad (42)$$

where

$$\kappa_r + j \kappa_i = \frac{1}{2 T_d} \sqrt{(1 + j T_d \omega_1)^2 - 4 T_d \alpha_c}. \quad (43)$$

The frequency response of the VSC equivalent impedance for the positive- and negative-sequence is

$$Z_{vsc}(\pm j\omega) = Y_{vsc}^{-1}(\pm j\omega) = \frac{L_f}{T_d} \pm j L_f \left(\omega \pm \omega_1 - \frac{\alpha_c}{T_d \omega} \right), \quad (44)$$

and the resonance frequencies are

$$\mathrm{Im}\{Z_{vsc}(\pm j\omega)\} = 0 \quad \Rightarrow \quad \omega_\pm = \sqrt{\left(\frac{\omega_1}{2} \right)^2 + \frac{\alpha_c}{T_d}} \mp \frac{\omega_1}{2}. \quad (45)$$

The poles and the resonance frequency in the $\alpha\beta$-frame become

$$s_1 = -\frac{1}{2 T_d} + \kappa_r + j \left(\kappa_i + \frac{\omega_1}{2} \right)$$

$$s_2 = -\frac{1}{2 T_d} - \kappa_r - j \left(\kappa_i - \frac{\omega_1}{2} \right) \quad (46)$$

$$\omega_\pm = \pm \frac{\omega_1}{2} + \sqrt{\left(\frac{\omega_1}{2} \right)^2 + \frac{\alpha_c}{T_d}}.$$

It can be observed that the system poles are not complex conjugate and the resonance frequency is different for the positive- and negative-sequence due to the feedforward complex gains introduced in the current control loop (e.g., the feedforward term $j L_f \omega_1 \mathbf{i}$) and the frequency translation.

APPENDIX B

THE VSC AND GRID INDUCTIVE AND CAPACITIVE RESPONSE

Considering that $G_i(\omega) << B_i(\omega)$ for $i = g$ and vsc, (18) can be approximated as $L(j\omega) \approx B_{vsc}(\omega) / B_g(\omega)$. Therefore,

$$\frac{d|L(j\omega)|}{d\omega} \approx \frac{\dfrac{1}{|B_g(\omega)|} \dfrac{d|B_{vsc}(\omega)|}{d\omega} - |B_{vsc}(\omega)| \dfrac{d|B_g(\omega)|}{d\omega}}{|B_g(\omega)|^2}. \quad (47)$$

From (47), the two cases of the second stability condition, (21) and (22), can be identified with the following parallel resonance situations:

- Case #1: Inductive response of the grid and capacitive response of the VSC, i.e.,

$$\frac{d|B_g(\omega)|}{d\omega} < 0 \quad \text{and} \quad \frac{d|B_{vsc}(\omega)|}{d\omega} > 0 \quad \Rightarrow \quad \frac{d|L(j\omega)|}{d\omega} > 0. \quad (48)$$

- Case #2: Capacitive response of the grid and inductive response of the VSC, i.e.,

$$\frac{d|B_g(\omega)|}{d\omega} > 0 \quad \text{and} \quad \frac{d|B_{vsc}(\omega)|}{d\omega} < 0 \quad \Rightarrow \quad \frac{d|L(j\omega)|}{d\omega} < 0. \quad (49)$$

REFERENCES

[1] B. Bahrani, *Advanced control strategies for voltage source converters in microgrids and traction networks*, (http://infoscience.epfl.ch/record/181221/files/EPFL_TH5479.pdf), PhD Degree Thesis in Energy, École Polytechnique Féderale de Lausanne, Switzerland, 2011.

[2] A. Yazdani and R. Iravani, *Voltage-sourced converters in power systems. Modeling, control and applications*, John Wiley & Sons, 2010.

[3] L. H. Kocewiak, *Harmonics in large offshore wind farms*, (http://vbn.aau.dk/files/62660098/lukasz_kocewiak.pdf), PhD Degree Thesis in Electrical Engineering, Dep. of Energy Technology, Aalborg University, Denmark, 2012.

[4] L. Harnefors, X. Wang, A. G. Yepes, and F. Blaabjerg, "Passivity-based stability assessment of grid-connected VSCs – An overview," *IEEE Journal and Selected Topics in Power Electronics*, vol. 4, no. 1, pp. 116–125, March 2016.

[5] X. Wang, F. Blaabjerg and W. Wu, "Modeling and analysis of harmonic stability in an AC power electronics-based power systems," *IEEE Transactions on Power Electronics,* vol. 29, no. 12, pp. 6421-6432, Dec. 2014.

[6] E. Möllerstedt and B. Bernhardsson, "Out of control because of harmonics – An analysis of the harmonic response of an inverter locomotive," *IEEE Control Systems Magazine*, vol. 20, no. 4, pp. 70-81, Aug. 2000.

[7] F. D. Freijedo, S. K. Chaudhary, R. Teodorescu, J. M. Guerrero, C. L. Bak, L. H. Kocewiak, and C. F. Jensen, "Harmonic resonances in wind power plants: modeling, analysis and active mitigation methods," *Proc. of the IEEE PowerTech Eindhoven*, June-July 2015, pp. 1-6.

[8] L. P. Kunjumuhammed, B. C. Pal, C. Oates, and K. J. Dyke, "Electrical Oscillations in Wind Farm Systems: Analysis and Insight Based on Detailed Modeling," *IEEE Trans. Sustainable Energy*, vol. 7, no. 1, pp. 51-62, Jan. 2016.

[9] B. Wen, D. Boroyevich, R. Burgos, P. Mattavelli and Z. Shen, "Small-signal stability analysis of three-phase AC systems in the presence of constant power loads based on measurements d-q frame impedances,"*IEEE Transactions on Power Electronics*, vol. 30, no. 10, pp. 5952-5963, Oct. 2015.

[10] J. Sun, "Impedance-based stability criterion for grid-connected inverters," *IEEE Transactions on Power Electronics*, vol. 26, no. 11, pp. 3075–3078, Nov. 2011.

[11] M. Céspedes and J. Sun, "Impedance modelling and analysis of grid-connected voltage-source converters," *IEEE Transactions on Power Electronics*, vol. 29, no. 3, pp. 1254–1261, Nov. 2014.

[12] M. Céspedes and J. Sun, "Impedance shaping of three-phase grid parallel voltage-source converters," 27th Annual IEEE Applied Power Electronics Conference and Exposition (APEC 2012)*,* Feb. 2012, pp. 754–760.

[13] L. Harnefors, L. Zhang, and M. Bongiorno, "Frequency-domain passivity-based current controller design," *IET Power Electronics*, vol. 9, no. 3, p. 1254-1261, 2014.

[14] L. Harnefors, M. Bongiorno and S. Lundberg, "Input-admittance calculation and shaping for controlled voltage-source converters," *IEEE Trans. on Industrial Electronics*, vol. 54, no. 6, pp. 3323-3334, Dec. 2007.

[15] I. M. Canay, "A novel approach to the torsional interaction and electrical damping of the synchronous machine, Part I: Theory," *IEEE Trans. Power App. Syst.*, vol. PAS-101, no. 10, pp. 3630–3638, Oct. 1982.

[16] I. M. Canay, "A novel approach to the torsional interaction and electrical damping of the synchronous machine, Part II: Application to an arbitrary network," *IEEE Trans. Power App. Syst.*, vol. PAS-101, no. 10, pp. 3639–3647, Oct. 1982.

[17] A. Tabesh and R. Iravani, "On the application of the complex torque coefficients method to the analysis of torsional dynamics," *IEEE Trans.Energy Convers.*, vol. 20, no. 2, pp. 268–275, Jun. 2005.

[18] L. Harnefors, "Analysis of subsynchronous torsional interaction with power electronic converters," *IEEE Trans. on Power Systems*, vol. 22, no. 1, pp. 305-313, Feb. 2007.

[19] L. Harnefors, "Proof and application of the positive-net-damping stability criterion," *IEEE Trans. on Power Systems*, vol. 26, no. 1, pp. 481-482, Feb. 2011.

[20] G. Stamatiou and M. Bongiorno, "Stability Analysis of Two-Terminal VSC-HVDC Systems using Net-Damping Criterion," *IEEE Trans. on Power Delivery*, vol. 31, no. 4, pp. 1748-1756, August 2016.

[21] C. Zhang, M. Molinas and A. Rygg, "Properties and Physical Interpretation of the Dynamic Interactions between Voltage Source Converters and Grid: Electrical Oscillation and Its Stability Control," *IET Power Electronics*, early access, http://dx.doi.org/10.1049/iet-pel.2016.0475.

[22] M. Zhao, X. Yuang, J. Hu. and Y. Yan, "Voltage dynamics of current control time-scale in a VSC-connected weak grid," *IEEE Transactions on Power Systems*, vol. 31, no. 4, pp. 2925-2937, July 2016.

[23] L. Harnefors, "Modeling of Three-Phase Dynamic Systems Using Complex Transfer Functions and Transfer Matrices," *IEEE Transactions on Industrial Electronics,* vol. 54, no. 4, pp. 2239-2248, Aug. 2007.